Pharmacological Research 194 (2023) 106844

Contents lists available at ScienceDirect

Pharmacological Research

journal homepage: www.elsevier.com/locate/yphrs

Multi-dimensional characterization of immunological profiles in small cell lung cancer uncovers clinically relevant immune subtypes with distinct prognoses and therapeutic vulnerabilities

Lin Yang [a,1], Zicheng Zhang [b,1], Jiyan Dong [a], Yibo Zhang [b], Zijian Yang [b], Yiying Guo [c], Xujie Sun [a], Junling Li [c], Puyuan Xing [c,*], Jianming Ying [a,*], Meng Zhou [b,*,2]

[a] Department of Pathology, National Cancer Center/National Clinical Research Center for Cancer/Cancer Hospital, Chinese Academy of Medical Sciences and Peking Union Medical College, Beijing 100021, PR China
[b] School of Biomedical Engineering, Eye Hospital, Wenzhou Medical University, Wenzhou 325027, PR China
[c] Department of Medical Oncology, National Cancer Center/National Clinical Research Center for Cancer/Cancer Hospital, Chinese Academy of Medical Sciences and Peking Union Medical College, Beijing 100021, PR China

ARTICLE INFO

Keywords:
Digital spatial profiling
Immune subtypes
Small cell lung cancer
Tumor microenvironment
Formalin-fixed-paraffin-embedded

ABSTRACT

Small-cell lung cancer (SCLC) is generally considered a 'homogenous' disease, with little documented inter-tumor heterogeneity in treatment guidance or prognosis evaluation. The precise identification of clinically relevant molecular subtypes remains incomplete and their translation into clinical practice is limited. In this retrospective cohort study, we comprehensively characterized the immune microenvironment in SCLC by integrating transcriptional and protein profiling of formalin-fixation-and-paraffin-embedded (FFPE) samples from 29 patients. We identified two distinct disease subtypes: immune-enriched (IE-subtype) and immune-deprived (ID-subtype), displaying heterogeneity in immunological, biological, and clinical features. The IE-subtype was characterized by abundant immune infiltrate and elevated levels of interferon-alpha/gamma (IFNα/IFNγ) and inflammatory response, while the ID-subtype featured a complete lack of immune infiltration and a more proliferative phenotype. These two immune subtypes are associated with clinical benefits in SCLC patients treated with adjuvant therapy, with the IE-subtype exhibiting a more favorable response leading to improved survival and reduced disease recurrence risk. Additionally, we identified and validated a personalized prognosticator of immunophenotyping, the CCL5/CXCL9 chemokine index (CCI), using machine learning. The CCI demonstrated superior predictive abilities for prognosis and clinical benefits in SCLC patients, validated in our institute immunohistochemistry cohort and multicenter bulk transcriptomic data cohorts. In conclusion, our study provides a comprehensive and multi-dimensional characterization of the immune architecture of SCLC using clinical FFPE samples and proposes a new immune subtyping conceptual framework enabling risk stratification and the appropriate selection of individualized therapy.

1. Introduction

Small-cell lung cancer (SCLC) has been regarded as a 'homogenous' disease, with patients receiving similar treatment approaches over the past few decades. Despite the addition of immunotherapy to platinum-based frontline chemotherapy, the improvements in overall response rate, progression-free survival, and overall survival have been minimal [1]. In contrast to non-small-cell lung cancer (NSCLC), where molecular

List of abbreviations: SCLC, Small-cell lung cancer; TME, Tumor microenvironment; TF, Transcriptional factor; NE, Neuroendocrine differentiation; TMB, Tumor mutation burden; DSP, Digital spatial profiling; FFPE, Formalin-fixed and paraffin-embedded; EMRS, Electronic medical record system; IHC, Immunohistochemistry; TMA, Tissue microarray; ROIs, Regions of interests; GEO, Gene Expression Omnibus; GSEA, Gene set enrichment analysis; CI, Confidence interval; HR, Hazard ratio; TGE, Targeted gene expression; TILs, Tumor-infiltrating lymphocytes.

* Corresponding authors.
E-mail addresses: xingpuyuan@cicams.ac.cn (P. Xing), jmying@cicams.ac.cn (J. Ying), zhoumeng@wmu.edu.cn (M. Zhou).
[1] Contribute equally to this work as the first authors.
[2] ORCID: 0000-0001-9987-9024

https://doi.org/10.1016/j.phrs.2023.106844
Received 15 March 2023; Received in revised form 27 June 2023; Accepted 28 June 2023
Available online 29 June 2023

stratification and predictive biomarkers have revolutionized treatment approaches, the underlying mechanisms driving therapeutic benefits in SCLC remain poorly understood [2]. Consequently, there is a lack of guidance for clinical research and the development of layered treatment strategies in SCLC.

The immune landscape within the tumor microenvironment has been widely recognized as a crucial determinant of prognosis and the anti-tumor immune response [2]. Our previous observational study in 247 resected SCLCs [3], along with the IMPower 133 [4] and CASPIAN [5] studies, demonstrated the potential for prolonged survival in a subset of SCLC patients through surgery or immune-based interventions. However, owing to technical limitations, previous studies have provided only a limited perspective on the immune microenvironment in SCLC, often focusing on a small number of specific cell types such as CD4 + or CD8 + T cells [6], tumor-associated macrophages, cancer-associated fibroblasts or particular gene signatures [7]. The impact of the immune landscape on prognosis and immune response is known to involve multiple specialized cell types that interact in a highly coordinated manner, as revealed in other cancer types [8–13]. However, the current understanding of the tumor immune landscape features of SCLC remains far more unclear [14]. Advancements in integrative multi-omics strategies have revolutionized therapeutic development for various tumor types [15–17]. Therefore, a comprehensive characterization of the immune landscape in SCLC is crucial for advancing therapeutic strategies and improving patient outcomes.

This study aims to elucidate the immunological architecture of SCLC through a multi-dimensional analysis incorporating targeted NanoString panel RNA sequencing, transcriptional profiling, and protein profiling and to understand the impact of the immunological architecture on prognosis and therapeutic clinical benefits. We identified immune-enriched (IE-subtype) and immune-deprived disease subtypes (ID-subtype) characterized by distinct immune features and clinical outcomes. Finally, we developed and validated a two-chemokine index (CCI) for immunophenotyping, which shows promise in the risk stratification of patients and aids in selecting personalized treatment strategies in clinical settings.

2. Methods and materials

2.1. Patient Cohorts and study design

This study was performed according to the Declaration of Helsinki and approved by the Ethics Committee of National Cancer Center/Cancer Hospital, Chinese Academy of Medical Sciences and Peking Union Medical College (approval NO.22/250–3452), and all patients have exempted an informed consent due to the retrospective nature. All data were anonymously analyzed.

In this retrospective study, the high-quality formalin-fixed and paraffin-embedded (FFPE) tumor tissues of 59 patients with resected limited-stage SCLC who received no chemo/radio-therapy before surgery were recruited between January 2009 and February 2016 from the archival electronic medical record system (EMRS) at the Department of Pathology, Cancer Hospital, Chinese Academy of Medical Sciences (CHCAMS).

The clinicopathologic information of 59 SCLC patients (e.g., age, gender, smoking history, tumor location, tumor thrombosis, treatment modes, T stage, N stage, M stage, overall survival, disease-free survival, etc.) from EMRS was manually curated and compiled. Inclusion criteria for sample analysis were as follows: (i) histological confirmation of pure SCLC without any combined histology after radical resection of lung cancer plus systemic lymph node dissection; (ii) limited stage classification according to the Veteran's Administration Lung Study Group's 2-stage classification scheme (VALSG) [18], and (iii) absence of synchronous or prior multiple primary lung cancer of other histology nor coexisting tumors from other organs. This study was designed with two cohorts: CHCAMS cohort-1, including 29 samples available for transcriptomic and proteomic profiling, and CHCAMS cohort-2, including 30 samples available for independent validation by immunohistochemistry (IHC).

2.2. RNA isolation and processing for customized neuroendocrine and immune signature

Archived FFPE blocks with sufficient tumor contents were collected for RNA extraction. Three Section (8 μm in thickness) were sectioned from each sample block. An additional tissue Sections (3–4 μm in thickness) from each sample was stained with H&E for pathological verification of the tumor region and border for macrodissection before RNA extraction. Total RNA was isolated using the RNeasy FFPE kit (Qiagen 73504) from fresh FFPE tumor sections and quantified using NanoDrop spectrophotometry (Thermo Fisher Scientific) and quality controlled using 2100 bioanalyzer (Agilent Technologies). RNA integrity was defined by the percentage of 300 ng with a passing threshold of 50% for digital counting using NanoString nCounter technology.

300 ng RNA of each sample extracted from corresponding FFPE tumor tissues from SCLC patients was analyzed on the NanoString nCounter system (NanoString Technologies, Seattle, WA, USA) using a custom-designed panel incorporating mRNA expression of 277 genes involved in immune checkpoint inhibitors, innate immunity, immune cell type biomarkers and neuroendocrine signature. After probe binding, the gene-specific fluorescence barcodes were hybridized, scanned, and quantified on the nCounter FLEX digital analyzer. Quality control (QC) and raw data processing were performed using the nSolver (v4.0.70). A binding density between 0.1 and 2.25 was regarded as good imaging QC and an R^2 over 0.95 of serial diluted spike-in positive controls was regarded as good internal QC for quantification. Raw data were normalized by the geometric mean of endogenous housekeeping genes. For further downstream analysis, normalized data were used directly as count values.

2.3. Acquisition and processing of whole transcriptional atlas and protein profiling for immune-oncology (I/O) targets

Transcriptional and protein profiling was generated using the NanoString GeoMx Digital Spatial Profiler (DSP) (NanoString, Seattle WA, USA) of 83 regions of interests (ROIs) from 29 resected SCLC as previously described [19]. All experiments were performed at Fynn Biotechnologies (Jinan, China). In general, the FFPE tissue section was deparaffinized and immunofluorescence-stained using Pan-CK (Novus NEP2–33200) and CD45 (CST13917) plus a nuclear stain SYTO13 (NanoString 121300310). Individual ROIs were selected to delineate cancer and infiltrating immune cells, respectively, with appropriate cell counts. A whole transcriptome atlas covering over 18,000 genes was used for transcriptional profiling. Hybridized probes were photocleaved by ultraviolet and oligonucleotide barcodes were collected and sequenced on an Illumina NovaSeq 6000 with a sequencing depth factor of 100 per μm^2. For protein profiling, experiments were carried out on a parallel-sectioned slide following the abovementioned process. Ultraviolet-photocleavable oligo-conjugated panel sets along with the above three visualization markers, containing 42 protein markers, were used for protein detection and quantification similarly upon ultraviolet-mediated illumination, target-specific oligo barcodes, details seen in NanoString Website (GeoMx DSP Configuration Files | NanoString).

The RNA data obtained underwent quality control checks and were normalized using the Q3 normalization method. The limit of quantitation (LOQ) of each ROI was determined using the formula: LOQ = Geomean (NegProbe) × GeoSD (NegProbe)^2. A total of 18,676 genes were included in the downstream analysis. For the assessment of the 42 proteins from the DSP immune-related panels or modules, the raw protein data were normalized using housekeeping proteins (Histone H3, GAPDH, RPS6) to eliminate inter-ROI expression bias and target

expression was also evaluated by comparison with three negative controls (mouse IgG1, mouse IgG2a, and rabbit IgG) before downstream analysis. Pseudo-bulk sequencing data for RNA and protein were generated by calculating the average expression levels of RNAs and proteins across all ROIs within each sample [20,21].

2.4. Public multicenter SCLC patient cohorts

A total of four multicenter SCLC patient cohorts with available transcriptomic data and clinical information were collected from the Gene Expression Omnibus (GEO) database and corresponding publications, including 50 patients from the GSE60052 cohort [22], 49 patients from George's study (George cohort) [23], 18 patients from the GSE149507 cohort [24] and 17 anti-PD-1/PD-L1 antibody-treated patients from Roper's study (Roper cohort) [25].

2.5. Functional and gene set enrichment analysis

Twenty-nine knowledge-based functional gene expression signatures (Fges) covering known immune, stromal, and other major cellular functional components of the tumor were obtained from Bagaev's study (Supplementary Table 1) [26]. Fifty hallmark gene sets were obtained from Molecular Signatures Database (MSigDB, v7.2) [27]. Gene set enrichment analysis (GSEA) was carried out by the R package 'clusterProfiler' (v4.2.2) [28]. The enrichment score (ES) of the GSEA method was used to calculate the enrichment level of specific gene sets or pathways. These ES scores were examined genes on the rank list from top to bottom. ES score was increased if a gene participated in the composition of the pathway or gene set, otherwise decreased. Normalized enrichment score (NES) was normalized to related pathways or gene set size. Positive NES represented the enrichment level at the top and negative NES represented the enrichment level at the bottom of the rank list. The single sample gene set enrichment analysis (ssGSEA) was performed using the R package 'GSVA' (v1.42.0) [29]. Enrichment analysis for gene ontology (GO) biological process gene sets was conducted by the ClueGO (plugin for Cytoscape software) [30].

2.6. Unsupervised clustering for molecular subtyping

The unsupervised consensus clustering analysis was applied to molecular data of SCLC tumor samples to identify potential molecular subtypes with the clustering number from 2 to 5 using the R package 'ConsensusClusterPlus' (v1.58.0) [31]. We selected the 80% item resampling (pItem), 1000 resamplings of 'reps', k-means method of 'clusterAlg' and Euclidean of 'distance' as the key input parameters on the consensus clustering models. The best consensus clustering k was chosen using the reference of cumulative distribution functions (CDF).

2.7. Immune infiltration estimations

Immune infiltration was computationally estimated using two immune cell gene signature-based methods, including the xCell method and the ssGSEA method. The xCell method (https://xcell.ucsf.edu/) was used to evaluate infiltrating levels of 64 immune and stroma cell types [32]. Twenty-eight immune cell gene sets were collected from previous publications (Supplementary Table 2) [33,34], and the ssGSEA method was used to quantify 28 infiltrating immune cells. We used the T cell exhaustion (TEX) signature [35], immune checkpoint inhibitory (ICI) signature [36,37] and cytotoxic signature to assess T cell dysfunction and exclusion level based on the ssGSEA method (Supplementary Table 3).

2.8. Identification and development of a 2-chemokine signature

To further investigate the interplay between immune subtypes in SCLC, we utilized an ensemble filtering pipeline among multi-platform expression profiles of 200 IFNγ pathway genes (Supplementary Table 4). First, expression levels of 200 IFNγ-related genes were compared between two immune subtypes from the NanoString panel profile with the Wilcoxon test. Genes with a P-value < 0.05 were considered statistically significant. The limma R package (v3.50.3) was used to identify differentially expressed genes. Genes with P-value$<$ 0.05 and fold-change (FC) > 1.5 were reserved to be statistically significant.

A 2-chemokine signature (CCL5/CXCL9 Index, CCI) was developed with the eXtreme Gradient Boosting machine-learning algorithm (XGBoost R package, v1.5.2.1). The kernel function of CCI was 'binary-logistic' and the max number of boosting iterations was 3000. To ensure the robust performance of the model, the tree depth was considered as 4, and the subsample ratio of training instance and columns in each tree were 50%. The evaluation metrics of validation data were displayed using 'error' on CCI. The CCI modeled via machine learning showed the best trade-off of predictive performance and model complexity. With CCI specified on the 0–1 index, the superior threshold was defined as 0.4 in the training cohort.

2.9. Immunohistochemistry (IHC) validation

IHC was performed on 4 μm thick full sections from selected blocks by fully automatic Roche immunohistochemical instruments (BenchMark ULTRA IHC/ISH System, Roche Diagnostics, BenchMark ULTRA system (roche.com)) according to the standard protocols. After deparaffinization, antigen retrieval of sections was at 97 °C for 30 min. Then sections were blocked in H_2O_2 at room temperature for 5 min and incubated at 4 ℃ overnight with primary antibodies against CXCL9 (ab9720, 1:100) and CCL5 (ab9679, 1:200), and incubated at room temperature with CD45(Kit-0024, MXB Biotechnologies) for 40 min, and then with HRP-labeled secondary antibody for 30 min at 37 °C. The interpretation of all IHC slides was completed by QuPath software v0.3.2 (https://qupath.github.io), an open-source and user-friendly software to evaluate and analyze digitally pathological characters on whole-slide imaging [38], for assessing via a combined score based on the intensity and the extent of staining under 200 × field microscopy.

2.10. Statistical analysis

All statistical analyses and graphical visualization were performed using R software (v4.1.3) and associated R packages. Tests involving categorical comparisons of distributions were performed using Fisher's exact tests, unless otherwise specified. Comparison between continuous variables was performed using Student's t-test or Wilcoxon rank-sum tests. The correlation between two continuous variables was determined by Pearson's correlation test. Univariable and multivariable Cox proportional hazards regression analysis was performed to evaluate the hazard ratio (HR) and 95% confidence interval (CI) of risk metrics with R package 'survival' (v3.4–0). The Kaplan-Meier survival curves and log-rank tests were performed to compare the survival difference between two and more groups using the R package 'survminer' (v0.4.9). The two-sided P-value < 0.05 was considered statistically significant.

3. Result

3.1. Integrated targeted gene expression (TGE) and whole transcriptome atlas (WTA) profiling identifies immune subtypes of SCLC

We conducted Pearson correlation analysis for NanoString targeted TGE profiling to identify co-expression patterns of pre-defined genes and biological activities using unsupervised hierarchical clustering and generated three major functional modules involved in the immune compartment, EMT and metabolic processes, and pro-tumor pathways in SCLC tumor microenvironment (Fig. 1 A and Fig. S1A). Remarkably, these three modules showed no obvious correlation with each other. To

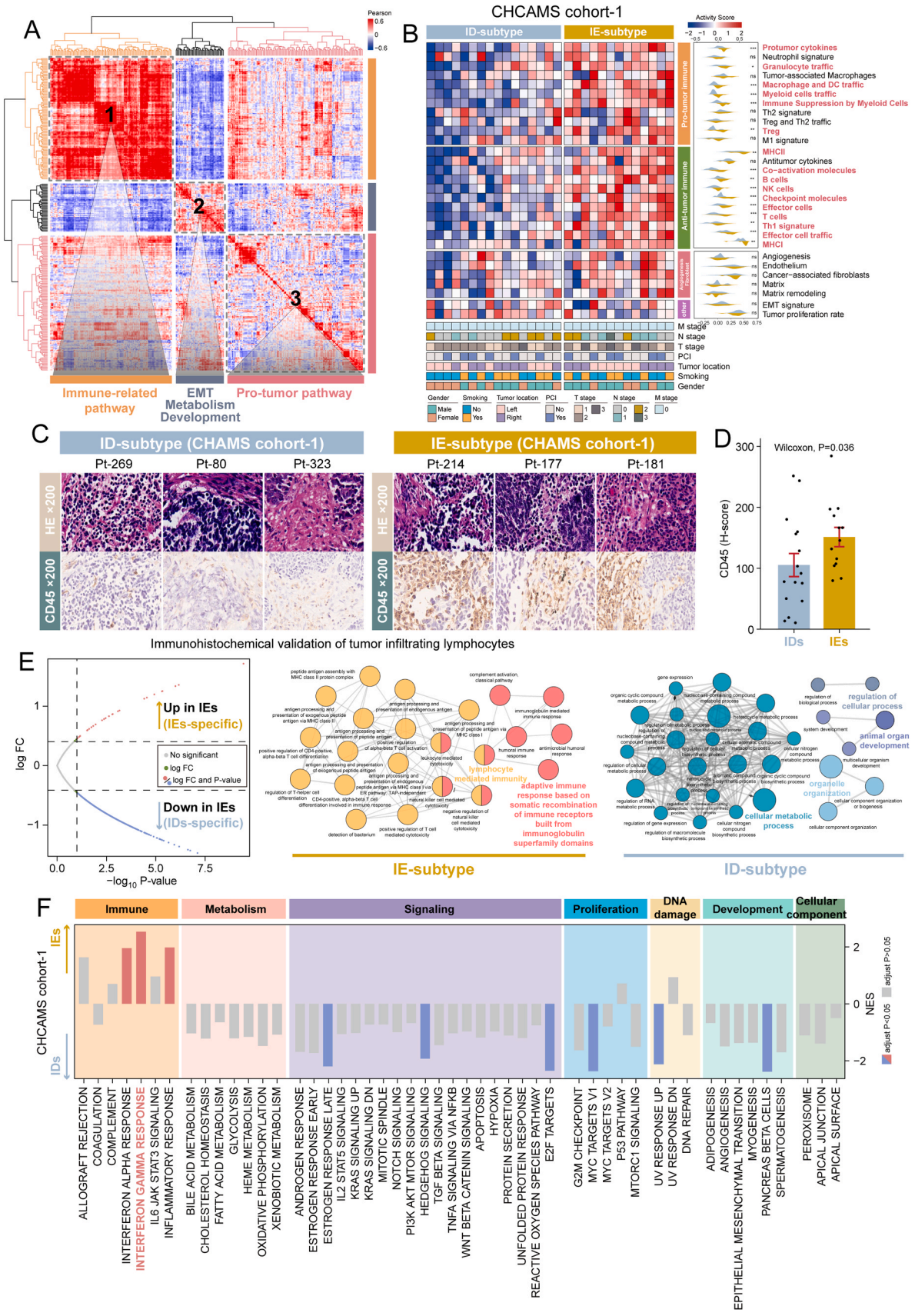

(caption on next page)

Fig. 1. Characterization of SCLC subgroups defined by immune gene profiling. (A) Unsupervised hierarchical clustering of the Pearson correlation matrix among genes from targeted gene expression profiling identifies three co-expression functional modules. (B) Heatmap of activity scores of 29 knowledge-based functional gene expression signatures (Fges) derived from single sample gene set enrichment analysis (ssGSEA) between IE-subtype and ID-subtype. The violin plot showed a distribution difference of 29 Fges activity scores between IE-subtype and ID-subtype. *P* value is calculated with the Wilcoxon test. (C) Representative hematoxylin and eosin (H&E) and IHC staining images of the two immune subtypes (200 × magnification). (D) Quantification of staining intensities for the indicated immune markers between IE-subtype and ID-subtype. Error bars represent mean ± SEM. *P* value is calculated with the Wilcoxon test. (E) Volcano plot showing differentially expressed genes (DEGs) between IE-subtype and ID-subtype (IE-subtype vs. ID-subtype). Red points represent overexpressed DEGs in IE-subtype and blue points under-expressed DEGs in IE-subtype. Green points represent only $|\log FC| > \log 1.5$ DEGs. Grey points represent insignificant DEGs. Network plot showing the enriched biological process in IE-subtypes and ID-subtype derived by Cytoscape plugin ClueGO. The *P*-value is calculated with the limma R package. (F) Bar plot depicting the enrichment scores of 50 hallmark gene sets between IE-subtype and ID-subtype.

further characterize the cellular and functional properties of the TME, we scored 29 Fges using ssGSEA from the whole transcriptomic profile. Unsupervised hierarchical clustering analysis of 29 Fges dichotomized 29 SCLC samples into two clusters with significantly varied immune compartments (Fig. 1B and Fig. S1B). One cluster can be characterized by higher levels of immune infiltrate, termed immune-enriched subtype (IE-subtype), compared with another cluster termed immune-deprived subtype (ID-subtype). However, there are no obvious differences in angiogenesis/fibroblast compartment, EMT signature, and tumor proliferation rate between IE-subtype and ID-subtype (Fig. 1B). Differences in the immune microenvironment between two clusters distinguished by our approach were also consistently observed when analyzing the abundance of tumor-infiltrating immune cells using 'xCell' method [32] or previously reported immune cell signatures by ssGSEA [33,34] (Fig. S1C). The gene signature expression pattern between immune subtypes is histologically correlated with lymphocyte spatial organization. IHC analysis in pathological sections also confirmed higher tumor-infiltrating lymphocytes (TILs) in IE-subtype compared with ID-subtype (mean H-score 151.24 vs. 105.29, $P = 0.036$) (Fig. 1C and D). Furthermore, immune subtyping identified in our cohort was also robustly reproduced in another public GSE149507 cohort (Fig. S1D-F), indicating that immune subtyping is duplicable and reliable.

We performed DE analysis between IE-subtype and ID-subtype to uncover the main biological features underlying immune subtypes. We found that immune-related processes, including lymphocyte-mediated immunity and adaptive immune response, were enriched in IE-subtype. In contrast, the cellular metabolic process, organelle organization, organ development and regulation of cellular process were enriched in ID-subtype (Fig. 1E). Pathway-level ssGSEA comparison analysis from 50 hallmark pathways obtained from MsigDB displayed that IE-subtype tumors featured by significantly enriched in IFN-α response, IFN-γ response and inflammatory response. Conversely, the E2F and MYC targets gene sets were significantly enriched in ID-subtype tumors, implying a more proliferative phenotype (Fig. 1 F). Similar results also were observed in the external GSE149507 cohort (Fig. S1G).

3.2. *Highly multiplexed digital spatial profiling reveals distinct T-cell infiltration and function in immune-enriched and immune-depleted SCLC*

The specific TGE and transcriptomic profiling does not uncover the spatial relationship and protein information for TILs in TME. Here, we quantitated the expression of 39 immuno-oncology proteins in 29 SCLC FFPE samples. We selected 83 ROIs in SCLC samples using fluorescent anti-CD45 (visualization marker for TIL ROIs) and anti-pan cytokeratin (PanCK, visualization marker for neoplastic epithelial cell ROIs) antibody (Fig. 2 A and Fig. S2). T cell scores, cytotoxicity scores, ICI scores and TEX scores (calculated as detailed in Methods) were higher in DSP CD45 + and CD3 + (markers for T cells) protein status than in CD45- and CD3- groups (Fig. 2B, C). Furthermore, gene expression and proteins for human IO drug target CD44 (R=0.62, $P < 0.001$) and human immune activation target IDO1 (R=0.49, $P = 0.007$) displayed a significant and positive association (Fig. S3A), serving as the validation for the CHCAMS cohort-1 gene expression based immune-related score.

Furthermore, we investigated the difference in co-localization patterns of 39 human IO proteins between CD3 + and CD3- SCLC samples (classified with the median split of barcode score). As shown in Fig. 2D, CD3 + T cells in immune-infiltrated FFPE co-localized with beta-2-microglobulin and immune-checkpoint target B7-H3 and T-cell immunoglobulin mucin family member 3 (Tim3). In contrast, the CD3- T cell group co-localized with signatures of inducible T-cell co-stimulator (CD11c) and CD44 (Fig. 2D). We further arranged each ROI into the immune-rich (CD45 hot spot, CD45 ++) or the immune-poor (CD45-/+) regimentation, utilizing the top and bottom quartile of CD45 barcode scores (Fig. 2E). When compared to immune-poor ROIs, CD45 + + immune-rich hot spot revealed significantly increased protein expression of CD3, CD4, CD8, immune-checkpoint targets and immune activation targets (Fig. 2 F).

When considered in aggregate protein expression patterns (29 samples, 83 ROIs and 39 IO proteins), we identified four protein modules to assess their correlations with clinical-biological functions. Abnormalities in module 2, module 3 and module 4 genes did not associate with specific tumor characteristics but correlated with immune activation, immune-checkpoint target, and cytotoxicity (Fig. S3B). In contrast, the proteins in module 1 were correlated with tumor proliferation and invasion, including B7-H3, CD56, Ki-67 and Histone H3. Meanwhile, up-regulated distribution in B7-H3, CD56, Ki-67 and Histone H3 were predominantly observed in CHCAMS cohort-1 SCLC patients with ID-subtype (Fig. S3C). Collectively, highly multiplexed ROIs of human IO proteins highlighted critical differences in TILs rich versus TILs poor subtypes and identified the tumor-related protein signatures in ID-subtype associated with more aggressive tumors.

3.3. *Immune subtypes are associated with clinical benefits in SCLC patients treated with adjuvant therapy*

To investigate the potential association between immune subtyping and the clinical efficacy of chemo/radio-therapy, we examined the disease-free survival (DFS) and disease recurrence rates in relation to the IE-subtype and ID-subtype. Survival analysis revealed notable differences in DFS between the two immune subtypes. Specifically, patients with the IE-subtype exhibited a more favorable clinical outcome, with a 3- and 5-year DFS rate of 69.2%. In contrast, patients with the ID-subtype demonstrated a less favorable prognosis, with a 3- and 5-year DFS rate of 46.7% and 37.3% (Fig. 3 A). Furthermore, the ID-subtype patients displayed a higher disease recurrence rate of 60% compared to those with the IE-subtype, who had a lower disease recurrence rate of 38.5% (Fig. 3B).

To further test the clinical relevance of the immune subtyping in SCLC immunotherapy, we recapitulated immune subtyping for 17 patients who received anti-PD-1/PD-L1 therapies in the Roper cohort (Fig. S4A, B), and observed that IE-subtype on Roper cohort shown substantially increased enrichment of immune-related pathways (Fig. 3 C). Notably, quantitative immune response review of Roper cohort revealed the IE-subtype was enriched with clinical benefit (CB) state (50%) and ID-subtype displayed a highest rate of no clinical benefit (NCB) state (81.8%) (Fig. 3 C). Among patients with prognostic comparison after immunotherapy, the Kaplan-Meier analysis revealed that IE-subtype patients achieved a significantly longer OS compared to ID-subtype patients (log-rank $P < 0.001$, Fig. 3D). Multivariable Cox regression analysis also indicated that the immune subtyping was

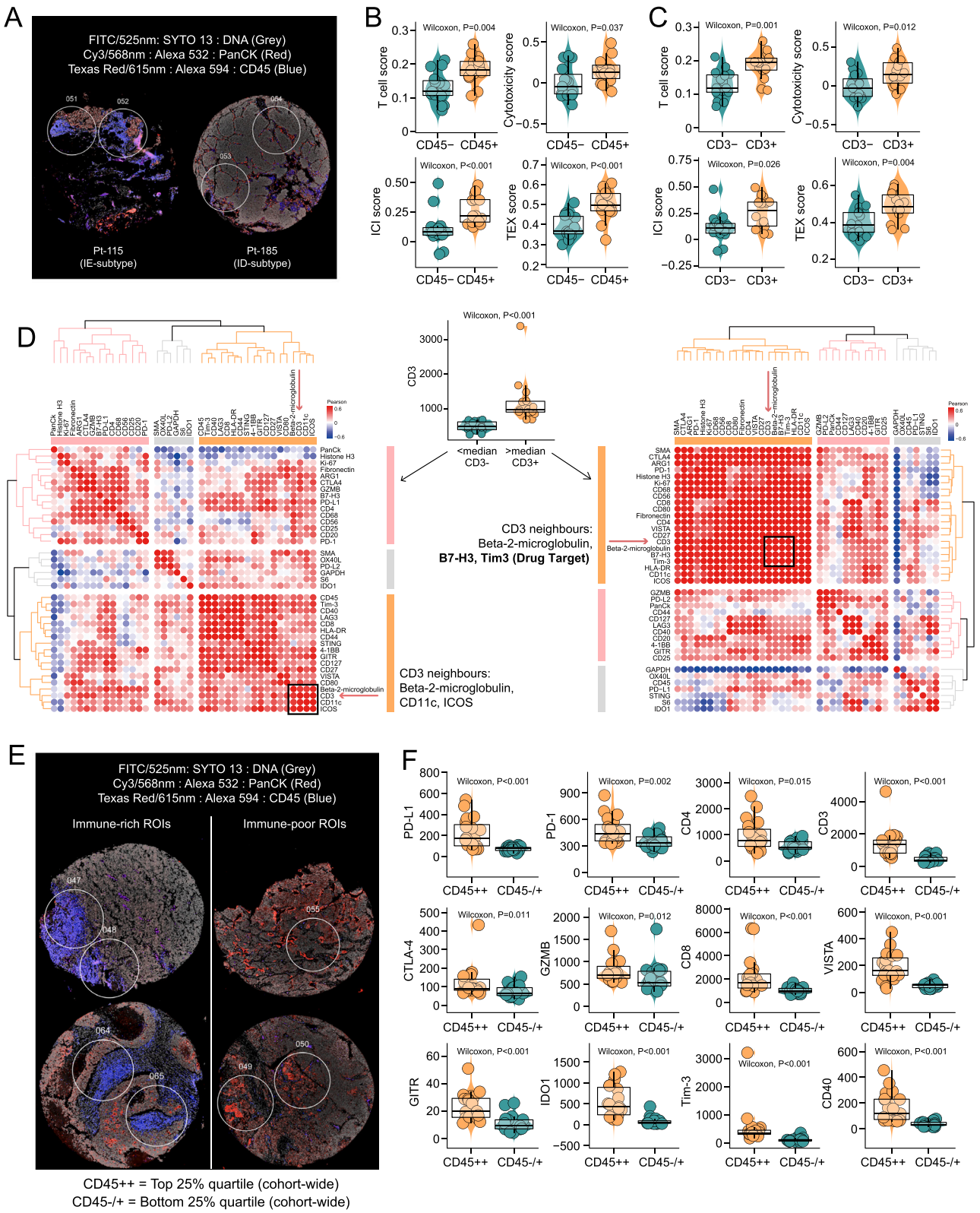

Fig. 2. Multiplexed protein detection with GeoMx DSP validates distinct T-cell infiltration and function between immune subtypes in SCLCs. (A) CD45 hotspots (blue fluorescence) in representative ROIs from SCLC FFPE sample. (B, C) Box plots showing the monotonic association of T cell score, cytotoxicity score, ICI score and TEX score between CD45 + and CD45- groups, and between CD3 + and CD3-groups. *P* value was calculated with the Wilcoxon test. (D) Unsupervised hierarchical clustering of 39 human IO proteins detected with GeoMx DSP showed the CD3 neighbors in 29 SCLC FFPE samples with high and low T-cell infiltration groups (median split). (E) CD45 hotspots (blue fluorescence) in representative regions of interest (ROIs). ROIs (n = 83) were assigned to either the immune-rich (CD45 "hotspot"; top 25% quartile of CD45 barcode scores) or the immune-poor category (bottom 25% quartile of CD45 barcode scores). (F) Box plots showing protein expression levels of PD-L1, PD-1, CD4, CD3, CTLA4, GZMB, CD8, VISTA, GITR, IDO1, Tim-3 and CD40 between CD45 + + and CD45-/+ subtypes. *P* value is calculated with the Wilcoxon test.

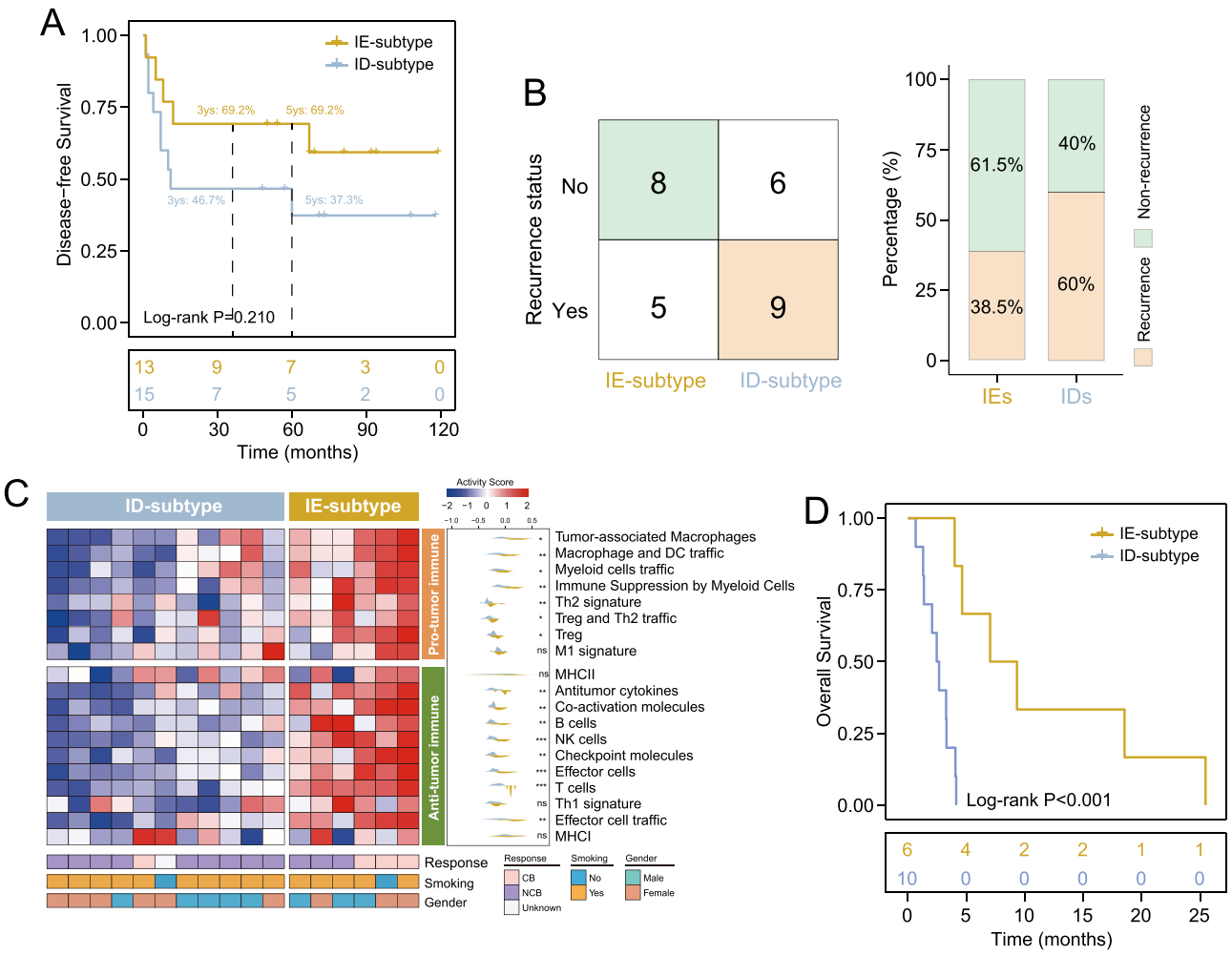

Fig. 3. Clinical relevance of immune subtyping in SCLC patients. (A) Kaplan-Meier curves for disease-free survival based on immune subtypes in the CHCAMS cohort-1. *P* value is calculated with the log-rank test. (B) The proportional distribution of recurrent and non-recurrent patients between IE-subtype and ID-subtype in the CHCAMS cohort-1. (C) Heatmap of scaled activity scores of pro-tumor immune and anti-tumor immune pathways between IE-subtype and ID-subtype in Roper cohort (immunotherapy). Violin plot showing the difference of pro-tumor immune and anti-tumor immune pathways between IE-subtype and ID-subtype. *P* value is calculated with the Wilcoxon test. (F) Kaplan-Meier curves for overall survival between IE-subtype and ID-subtype in the Roper cohort (immunotherapy). *P* value is calculated with the log-rank test.

retained as an independent immunotherapy prognostic factor for OS (HR=0.054, 95% CI 0.005–0.552, $P = 0.014$, Fig. S4C). These findings underscore the potential impact of immune subtyping on the clinical efficacy of chemo/radio-therapy or immunotherapy in SCLC patients.

3.4. A CCL5/CXCL9 chemokine index as a personalized prognosticator of immunophenotyping for clinical translation

The above hallmark gene set analyses indicated that IFN-γ response is most significantly enriched in IE-subtype, highlighting the key contribution of IFN-γ pathway activation to differential functional states of the two immune types. Prompted by the above observations, we used multi-platform profiles and a filtering pipeline algorithm to discover the shared axis on 200 IFNγ-related genes (Fig. 4 A). We found that the expression of two specific chemokines (CCL5 and CXCL9) was significantly associated with the immune subtyping. These two chemokines were significantly upregulated in IE-subtype SCLC samples relative to ID-subtypes, which was further validated in the external GSE149507 cohort (Fig. 4B). These results indicated that expression levels of CCL5 and CXCL9 denoted a main difference in immune properties for the two immune subtypes. Therefore, we defined a computational index for the CCL5/CXCL9 chemokine axis (CCI) as a personalized prognosticator of immune subtyping for clinical translation. The CCI dichotomized SCLC cases into a high CCI (CCI^{hi}) group and low CCI (CCI^{lo}) group using 0.4 as a threshold for representing the IE-subtype and ID-subtype. We next tested the prognostic value of the CCI using multicenter bulk transcriptomic cohorts. The Kaplan-Meier analysis revealed that the CCI^{hi} cases were associated with superior prognosis and prolonged patient survival time compared to CCI^{lo} cases across different cohorts (log-rank $P = 0.051$ for the GSE60052 cohort, $P = 0.076$ for the George cohort and $P = 0.074$ for CHCAMS cohort-1) (Fig. 4 C). Furthermore, the CCI also displayed robust and excellent prognostic value in SCLC immunotherapeutic patients. The CCI^{lo} cases in the Roper cohort were also correlated with inferior prognosis and shortened patient survival (log-rank $P = 0.001$, Fig. 4D).

To determine whether the CCI could be utilized as a prognostic tool in the clinical application using IHC quantitative profile, we re-collected other 30 SCLC patients' FFPE sample and clinical information (CHCAMS cohort-2, IHC) as shown in Fig. 4E, and measured protein expression of CCL5 and CXCL9 using the quantitative computerized IHC analysis for experimental verification at the protein level. Using the H-score of CCL5 and CXCL9 from the quantitative analysis as input, the CCI stratified 30 patients into CCI^{hi} (n = 12) and CCI^{lo} (n = 18) groups (Fig. 4E). As expected, tumors in the CCI^{hi} group showed significantly higher CCL5 (Wilcoxon, $P < 0.001$) and CXCL9 (Wilcoxon, $P = 0.003$) protein expression than cases in the CCI^{lo} group (Fig. 4 F, G). As indicated by the

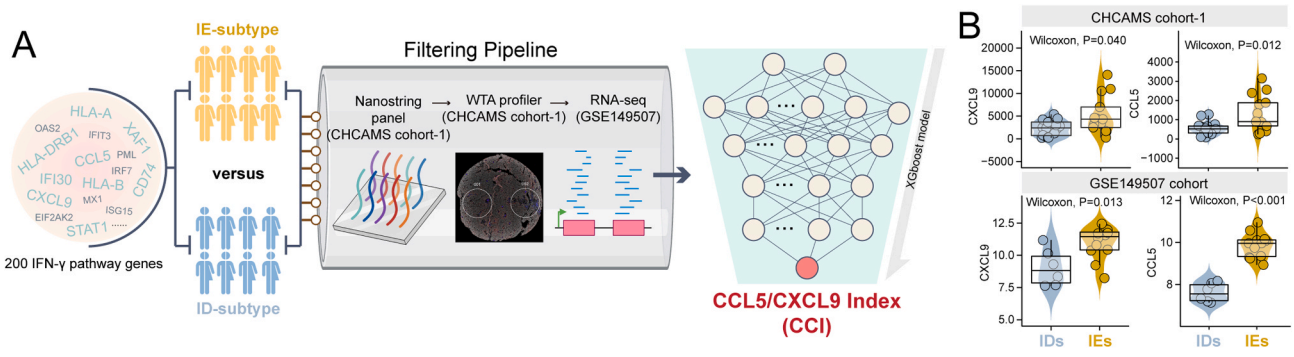

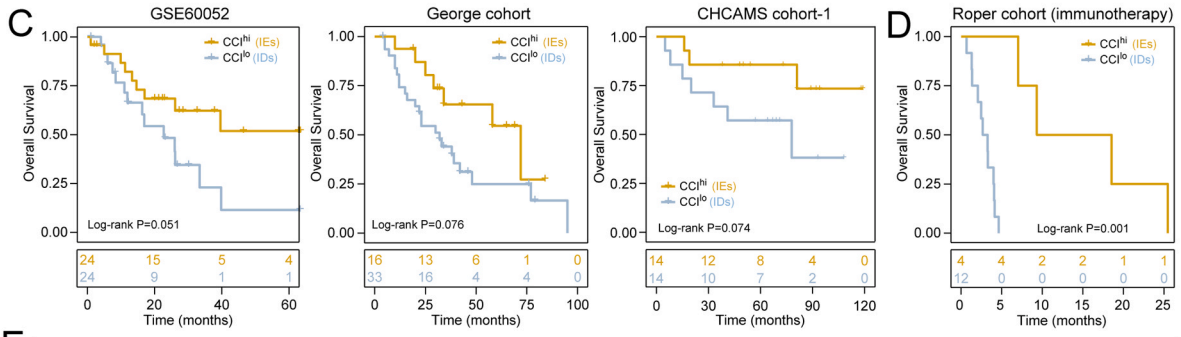

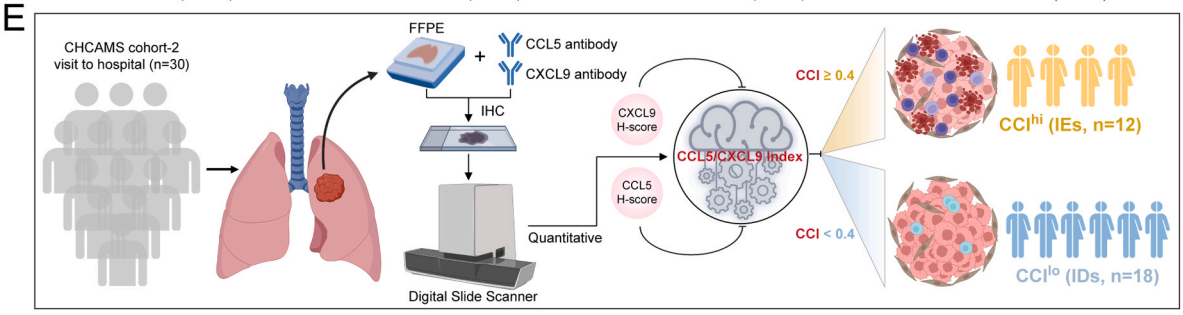

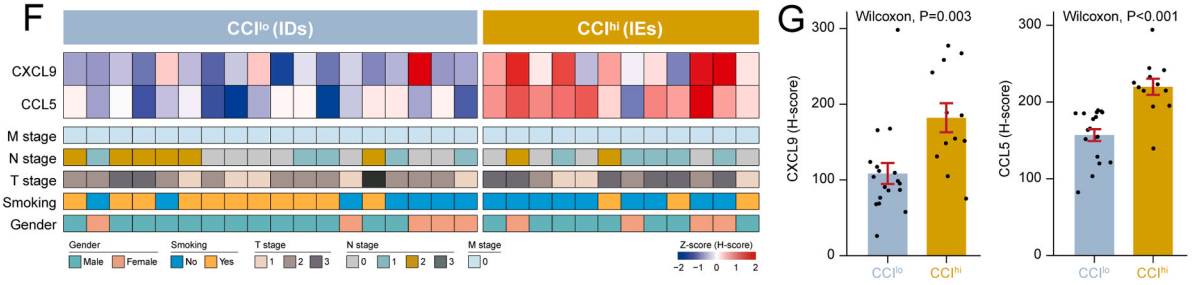

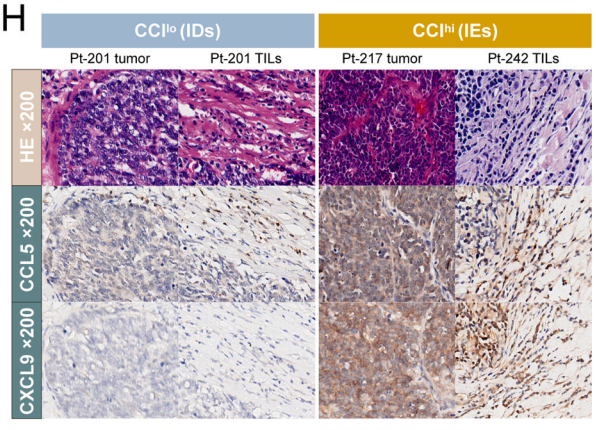

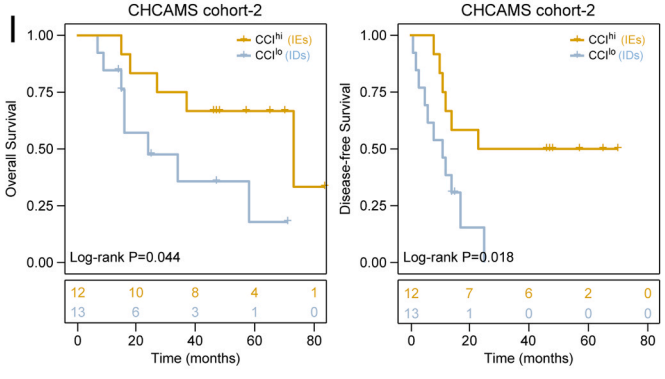

(caption on next page)

Fig. 4. A two-chemokine (CCL5/CXCL9) index (CCI) is a robust and personalized prognosticator in SCLC. (A) Workflow for identifying CCL5/CXCL9 chemokine Index (CCI). (B) Box plots showing expression levels of CCL5 and CXCL9 between IE-subtype and ID-subtype in CHCAMS cohort-1 and GSE149507 cohort. *P* value is calculated with the Wilcoxon test. (C, D) Kaplan-Meier curves for overall survival between risk groups stratified by the CCI in multicenter SCLC cohorts. *P* value is calculated with the log-rank test. (E) Workflow for validating the CCI in recollected SCLC cohort through the quantitative computerized immunohistochemistry analysis at the protein level (CHCAMS cohort-2, n = 30). (F) Heatmap of scaled H-scores of CCL5 and CXCL9 chemokines and clinical features between CCI^{hi} and CCI^{lo} groups. (G) Bar plot showing the protein levels of CCL5 and CXCL9 between CCI^{hi} and CCI^{lo} groups. Error bars represent mean ± SEM. *P* value is calculated with the Wilcoxon test. (H) Representative hematoxylin and eosin (H&E) and CCL5 and CXCL9 IHC staining images (200 × magnification). (I) Kaplan-Meier curves for the overall survival and disease-free survival between risk groups stratified by the CCI in the CHCAMS cohort-2 (IHC).

representative IHC image in the SCLC sample, the protein expression of CCL5 and CXCL9 almost exclusively and was commensurate with each other in the CCI^{hi} group, while the density of CCL5 and CXCL9 were low in the CCI^{lo} group both for tumor cells and TILs (Fig. 4H). In line with the results of bulk transcriptomic cohorts, the CCI assisted in survival prediction and allowed the identification of patient subgroups with good or poor outcomes in the CHCAMS cohort-2 cohort. Kaplan-Meier analysis showed that tumors in the CCI^{hi} group were significantly associated with superior prognosis and prolonged survival in terms of OS (log-rank $P = 0.044$) and DFS (log-rank $P = 0.018$, Fig. 4I) relative to cases in the CCI^{lo} group. Multivariaable Cox regression analyses also indicated that the CCI is an independent predictor of patients' prognosis after being adjusted by clinicopathologic characteristics in multiple bulk transcriptomic cohorts and IHC cohorts (Table 1). Together, these results experimentally confirmed the stability and reliability of the CCI, and validated the translational relevance of the CCI as a promising predictive tool.

3.5. Immune subtypes stratify SCLC patients and differ across NE subtypes and TF subtypes

To investigate the association of immune subtyping with previously reported TF subtyping and NE subtyping in SCLC tumors, we conducted an analysis using a meta-cohort of 145 SCLC samples through merging CHCAMS cohort-1, GSE60052 cohort, George cohort and Roper cohort used in this study. We categorized the samples into the six traditional subtypes previously reported in studies [37,38]: SCLC-A, SCLC-N, SCLC-P, SCLC-Y, NE-high, and NE-low. Interestingly, we observed that patients in IE-subtype and ID-subtype belonging to the IE-subtype and ID-subtype were distributed across the different TF subtypes and NE subtypes (Fig. 5A). The ID-subtype showed a predominant presence of SCLC-A (78.05%), SCLC-N (15.85%), and NE-high (92.68%) subtypes. In contrast, the IE-subtype not only exhibited enrichment in SCLC-A (66.67%), SCLC-N (14.29%), and NE-high (60.32%) subtypes but also displayed an increased population of SCLC-P (14.29%) and NE-low (39.68%) subtypes (Fig. 5A).

To further assess the prognostic significance of the CCI across traditional SCLC subtypes, the stratification analysis was performed in meta-cohorts (N = 145). Survival analysis revealed that CCI^{hi} tumors in both NE-high (log-rank $P = 0.014$) or NE-low (log-rank $P = 0.010$) subtypes exhibited significantly better survival compared to CCI^{lo} tumors (Fig. 5B, C). Among the TF subtypes, patients in the SCLC-A subtype demonstrated a more pronounced benefit from CCI^{hi}, as evidenced by significantly prolonged OS compared to those in the CCI^{lo} group (log-rank $P = 0.009$, Fig. 5D). Moreover, CCI^{hi} tumors in the SCLC-N, SCLC-P and SCLC-Y subtypes showed a strong trend toward improved OS compared to CCI^{lo} tumors (3ys: 71.4% and 5ys: 71.4% in SCLC-N CCI^{hi} versus 3ys: 38.5% and 5ys: 23.1% in SCLC-N CCI^{lo}; 3ys: 85.7% and 5ys: 68.6% in SCLC-P CCI^{hi} versus 3ys: 50% and 5ys: 50% in SCLC-P CCI^{lo}), although statistical significance was not reached, likely due to the limited sample size (Fig. 5E-G). These findings highlight the robust prognostic value of the CCI across TF subtyping and NE subtyping in SCLC.

4. Discussion

Using multicenter SCLC cohorts and multi-dimensional molecular profiling, the current study unveiled and experimentally validated the underlying immune heterogeneity of SCLC that stratified patients into immune subtypes for assisting prognosis and therapeutic predictions. We used multi-dimensional analysis of RNA sequencing and protein quantification to identify IE-subtype and ID-subtype characterized by distinct immune features and clinical outcome of prognosis and therapeutic efficacy. Specifically, we finally defined a two-chemokine index CCI to differentiate IE-subtype and ID-subtype by IHC, which is of great potential for patient risk stratification and selection of beneficiaries for immunotherapy. To our knowledge, this is the first comprehensive multi-dimensional study of the immune microenvironment in SCLC by using clinical FFPE samples for integrating transcriptomics and protein expression analysis.

Although ICIs have revolutionized cancer care, durable responses are observed only in a minority of patients, sometimes at the cost of severe toxicities. The same happens in SCLC, especially in unselected patients [39]. Therefore, the a priori identification of responders would improve clinical outcomes and is critically needed [39]. Here, we show that immune classification of IE-subtype and ID-subtype can further stratify patients with survival and responses to chemo-or chemo-plus immunotherapy. The immune classification in this study is superior to the traditional NE and TF subtypes in differentiating prognosis and treatment response. As compared with the immune subtypes, neither the NE subtype nor the TF subtype can fully distinguish the immune status of SCLC [40], although NE-low SCLCs are associated with increased immune cell infiltration (i.e., CD45 +, CD3 +, and CD8 + cells), which can be called "hot" or "immune oasis" phenotype as compared to NE-high tumors with an "immune desert" phenotype [41]. Our immune subtype is unique in that it can distinguish the prognosis in each subgroup of NE and TF with better adaptability and robustness than the traditional NE and TF subgroups [42].

We defined two distinct immune subtypes utilizing unsupervised hierarchical clustering analysis of transcriptomics data of SCLC from the archival FFPE clinical samples. Compared to previous research based on frozen tissue samples, cell lines, or xenografts [34], our immune classification is closer to real-world clinical pathological conditions, and the CCI we developed is more suitable for further clinical verification. Like other malignancies, SCLC exhibits a highly versatile network with inherent complexity in the tumor microenvironment, composed of cancer cells, immune cells, and supporting cells, along with a wide range of metabolites and cytokines. It has been confirmed that tumor cells can influence the immune contexture by expressing cell membrane-associated coinhibitory receptors or secreting various soluble factors to modulate certain immune subsets, shaping the tumor microenvironment into an immunosuppressive landscape [43]. Therefore, firstly, we developed a customized mRNA panel of 277 genes tested on Nanostring nCounter and identified that the immune-related pathway was independent of the pro-tumor pathway and EMT/Metabolism development, which indicated that tumor parenchyma (cancer cells) and immune stroma play a relatively independent role in the pathogenesis and evolution of SCLC. It is theoretically feasible to focus on the research of prognostic grouping strategy based on tumor-promoting and tumor-suppressing immunity characteristics. We also discovered the underlying transcriptomic features that stratify SCLC into IE-subtype and ID-subtype, and validated in different cohorts of bulk RNA sequencing and IHC for prognosis and treatment efficacy, reinforcing the notion and robustness of our immune subtypes that

Table 1
Multivariaable Cox analysis of overall survival and disease-free survival among SCLC bulk transcriptomic and IHC cohorts.

Cohorts	Variables	HR	95% CI	*P*-value
GSE60052 (overall survival)	**CCI:** Low (reference)			
	High	0.400	0.16–1.001	0.050
	Age	1.002	0.956–1.050	0.945
	Gender: Female (reference)			
	Male	0.224	0.032–1.583	0.134
	Smoking history: No (reference)			
	Yes	3.003	0.654–13.781	0.157
	T stage	1.326	0.744–2.364	0.338
	N stage	3.119	1.473–6.604	0.003
George cohort (overall survival)	**CCI:** Low (reference)			
	High	0.325	0.062 – 1.695	0.182
	Age	1.045	0.950–1.150	0.366
	Gender: Female (reference)			
	Male	0.542	0.107–2.735	0.458
	T stage	1.509	0.558–4.082	0.418
	N stage	1.586	0.700–3.591	0.269
CHCAMS cohort (overall survival)	**CCI:** Low (reference)			
	High	0.325	0.062–1.695	0.182
	Age	1.045	0.950–1.150	0.366
	Gender: Female (reference)			
	Male	0.542	0.107–2.735	0.458
	T stage	1.509	0.558–4.082	0.418
	N stage	1.586	0.700–3.591	0.269
CHCAMS IHC cohort (overall survival)	**CCI:** Low (reference)			
	High	0.253	0.065–0.984	0.047
	Age: < = 65 (reference)			
	> 65	4.618	0.863–24.714	0.074
	Gender: Female (reference)			
	Male	0.663	0.143–3.084	0.600
	T stage	1.328	0.517–3.408	0.555
	N stage	2.011	0.640–6.321	0.232
CHCAMS IHC cohort (disease-free survival)	**CCI:** Low (reference)			
	High	0.212	0.065–0.688	0.010
	Age: < = 65 (reference)			
	> 65	2.610	0.533–12.775	0.236
	Gender: Female (reference)			
	Male	1.259	0.340–4.667	0.730
	T stage	1.784	0.856–3.718	0.122
	N stage	0.796	0.265–2.390	0.685

unique immune molecular features can distinguish SCLC across TNM stages, smoking and gender, etc.[44]. IE-subtype exhibits significantly adaptive immune and lymphocyte-mediated immunity including antigen processing and presentation, positive regulation of CD4 +T cell differentiation involved in immune response, and leukocyte mediated cytotoxicity, etc., while ID-subtype has more metabolism, signaling, DNA damage, cell proliferation and development, etc. Specifically, IE-subtype exhibits significantly higher infiltrative pro-tumor and anti-tumor immune cells (like T cells, B cells, Macrophage, DC, myeloid cells, and checkpoint molecules, etc.), while no significant difference in angiogenesis, cancer-associated fibroblasts, matrix, and matrix remodeling, EMT signatures.

We validated the underlying transcriptomic stratification of ID-subtype and IE-subtype on a highly multiplexed DSP and revealed distinct T-cell infiltration in IE-subtype featured by significantly enriched in IFN-α response, IFN-γ response and inflammatory response, while ID-subtype enriched in the E2F and MYC targets gene sets. By histology, it can be seen that IE-subtype patients have higher infiltration of CD45 + lymphocytes in the tumor center, which has been confirmed as a favorable prognostic factor for resected SCLC [45]. Intriguingly, IE-subtype is enriched in T cell activity as can be seen that T cell score, cytotoxicity score, ICI score and TEX score are significantly higher in CD45 + and/or CD3 + patients than that of CD45- and/or CD3- cases. As for CD3 + patients, clustering analysis reveals more correlation with I/O target molecules such as B7-H3, Tim3, etc. Similar results are found in different ROIs stratified by CD45 that PD-L1, PD-1, CTLA-4, GZMB, VISTA, GITR, IDO1, Tim-3, and CD40 are significantly up-regulated with a higher expression of CD45. On the other hand, a higher expression of B7-H3, CD56, Histone H3 and Ki-67 is found in ID-subtype, and they are clustered into one functional module when all enrolled protein markers are analyzed, indicating that they contribute to a higher invasive nature of ID-subtype cases. B7-H3, also known as CD276, recently recovered from having an inhibitory ability towards both CD4 + and CD8 +T cells. In SCLC, B7-H3 is not associated with the level of CD3, CD8, or CD20 + TILs, but is correlated with tumor progression from both immunological and non-immunological aspects, and may contribute to the anti-cancer drugs resistance with various mechanisms [46]. And this is partly attributed to a higher recurrence and lower overall survival of the ID-subtype than that of IE-subtype.

Our immune subtyping can be helpful for predicting survival and selecting potential beneficiaries prior to therapy for the following reasons: [1] we found IE-subtype patients had significantly longer survival both for adjuvant radio/chemotherapy and immunotherapy; [2] we identified two specific chemokines(CCL5 and CXCL9) from IFN-γ pathway contributing to differential functional states of the two immune types; [3] we defined a computational index for the CCL5/CXCL9 chemokine axis (CCI) as a personalized prognosticator of immune subtyping for clinical translation. Furthermore, the CCI also displayed robust and excellent prognostic value in SCLC immunotherapeutic cohort patients. Recently, more attention has been paid to chemokines in SCLC for targets or modulators for augmenting the anti-tumor immune responses in chemo-/immune-therapeutic strategies [47]. As CC and CXC key members in highly dynamic and versatile chemokines networks in the tumor microenvironment, CCL5 and CXCL9 play an essential role in tumor progression, tumor-related inflammation and immunity. In solid tumors, co-expression of CCL5 and CXCL9 can promote T cell migration and recruitment, and be amplified by the INF-γ pathway, which makes the tumor cells reactive to ICIs and prolongs the survival period[48]. In SCLC, the expression of CCL5 positively correlates with patient survival and immune infiltration and can predict better ICB treatment response [49]. In NSCLC, high expression of CXCL9 in patients with more significant ICI immune response was confirmed by bronchoalveolar lavage fluid, suggesting that CXCL9 is a promising predictor for immunotherapeutic response [50]. Similar to lung cancer, CCL5 and CXCL9 are included in the four chemokines (CCL4, CCL5, CXCL9, and CXCL10) to form a T-inflamed phenotype in pancreatic cancer, which is correlated with a high expression of immune checkpoints (PD-L1, PD-1, and CTLA4, etc.) for the potential use of hierarchical markers for immunotherapy, similar as in hepatocellular carcinoma for predicting the efficacy of immunotherapy [51]. From a multi-dimensional perspective, our study has revealed the prognostic and immunotherapeutic biomarker

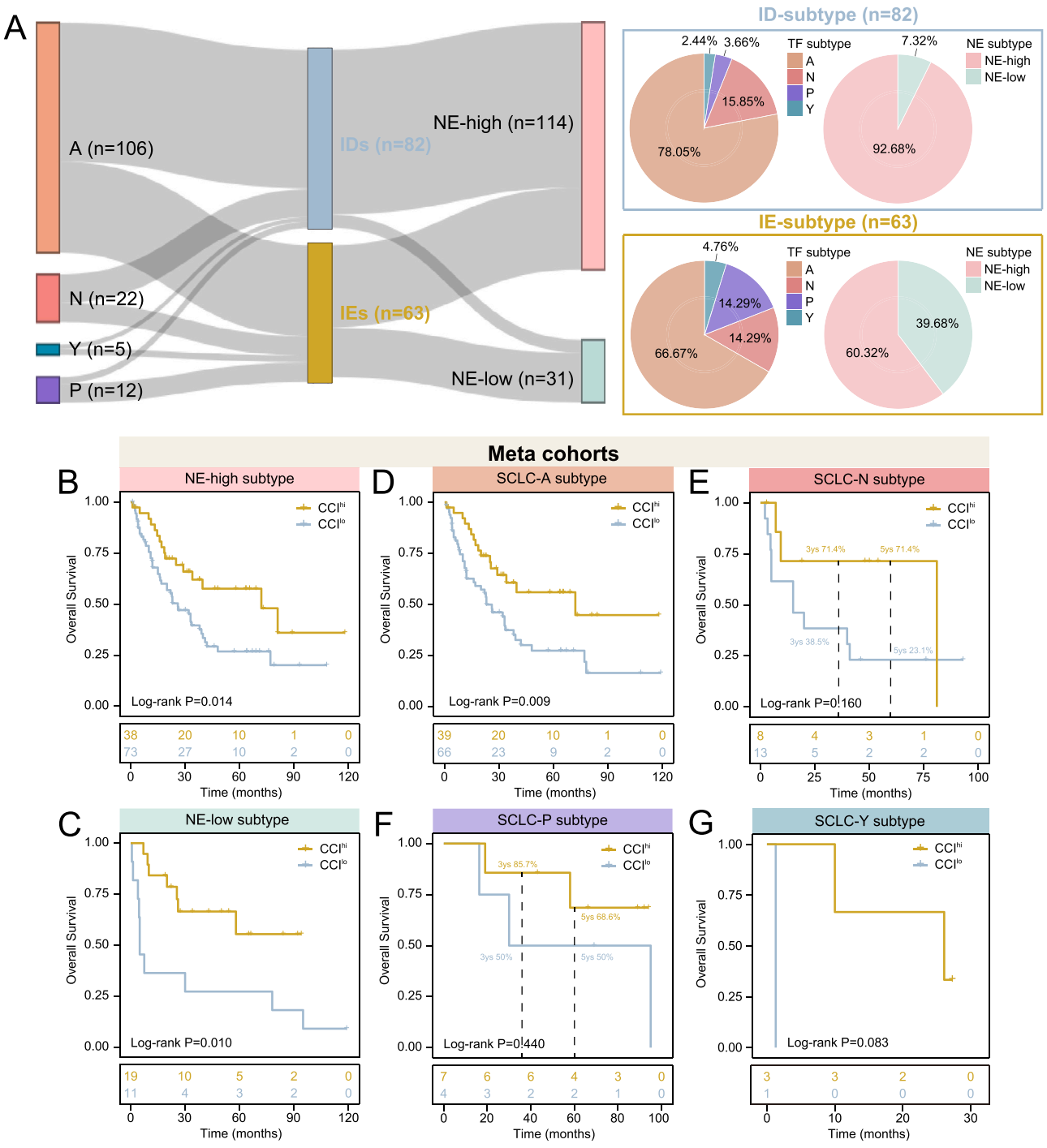

Fig. 5. Immune subtypes stratify SCLC patients and differ across the TF subtypes and NE subtypes. (A) Sankey diagram showing the crosstalk in the immune subtype and TF subtype and NE subtype. Pie plots showing the distribution of traditional molecular subtypes in IE-subtype and ID-subtype. (B-G) Kaplan-Meier curves for the overall survival between CCI^{hi} and CCI^{lo} groups within the stratification of TF subtype and NE subtype on meta-cohort. *P* value is calculated with the log-rank test.

potential of the CCL5/CXCL9 chemokine index in SCLC. Specifically, it has a promising clinical application in separating IDs and IEs before treatment. As per our definition, CCI depends on H-scores for CCL5 and CXCL9 at the immunohistochemical level. Therefore, accurately judging the immunohistochemical staining intensity and area remains challenging in clinical settings, especially for definitive CCI subtyping as CCI^{hi} or CCI^{lo}. To address this issue, strengthening the quality control of diagnostic physicians or utilizing artificial intelligence-assisted quantitative scoring may prove beneficial.

5. Conclusions

This study dissected the heterogeneity of the immune architecture of SCLC at high resolution and proposed a new immune subtyping conceptual framework to assess patient survival outcomes and therapeutic response enabling risk stratification and the appropriate selection of individualized therapy. To our knowledge, this is the first comprehensive multi-dimensional study of the immune microenvironment in SCLC using clinical FFPE samples with significant clinical application potential.

Funding

This study was supported by the Special Project for Clinical and Translational Medicine Research of Chinese Academy of Medical Sciences (2021-12M-C&T-B-062), the National Natural Science Foundation of China (Grant No.82172826), the Innovation Fund for Medical Sciences of Chinese Academy of Medical Sciences(2021-I2M-1-067)., and the Cancer Foundation of China, Beijing Hope Marathon Foundation (LC 2017 A20). The funders had no roles in the research design, conduct, analysis and manuscript production.

CRediT authorship contribution statement

Lin Yang: Conceptualization, Methodology, Investigation, Formal analysis, Project Administration, Writing – original draft, Funding acquisition, Writing – review & editing. **Zicheng Zhang:** Data curation, Methodology, Software, Formal analysis, Visualization, Writing – original draft. **Jiyan Dong:** Resources, Data curation, Writing – original draft; **Yibo Zhang:** Visualization, Formal analysis. **Zijian Yang:** Visualization, Formal analysis. **Yiying Guo:** Investigation, Resources, Data curation. **Xujie Sun:** Data curation, Validation. **Jinlin Li:** Methodology, Funding acquisition, Supervision; **Puyuan Xing:** Funding Acquisition, Writing – review & editing, Supervision. **Jianming Ying:** Funding acquisition, Writing – review & editing. **Meng Zhou:** Conceptualization, Supervision, Project administration, Formal analysis, Writing – review & editing.

Declaration of Competing Interest

The authors declare that they have no competing interest.

Data Availability

Data will be made available on request.

Acknowledgments

The graphic abstract was created using BioRender (www.biorender.com/).

Consent for publication

Not applicable.

Appendix A. Supporting information

Supplementary data associated with this article can be found in the online version at doi:10.1016/j.phrs.2023.106844.

References

[1] L. Horn, A.S. Mansfield, A. Szczęsna, L. Havel, M. Krzakowski, M.J. Hochmair, et al., First-line atezolizumab plus chemotherapy in extensive-stage small-cell lung cancer, New Engl. J. Med 379 (23) (2018) 2220–2229.
[2] T. Li, T. Qiao, Unraveling tumor microenvironment of small-cell lung cancer: implications for immunotherapy, Semin Cancer Biol. 86 (Pt 2) (2022) 117–125.
[3] S. Wang, Y. Li, Z. Liu, W. Tian, Y. Zeng, J. Liu, et al., Efficacy and safety of first-line immune checkpoint inhibitors combined with chemotherapy for extensive-stage small cell lung cancer: a network meta-analysis, Lung Cancer 178 (2023) 47–56.
[4] L. Horn, A.S. Mansfield, A. Szczesna, L. Havel, M. Krzakowski, M.J. Hochmair, et al., First-line atezolizumab plus chemotherapy in extensive-stage small-cell lung cancer, New Engl. J. Med 379 (23) (2018) 2220–2229.
[5] L. Paz-Ares, M. Dvorkin, Y. Chen, N. Reinmuth, K. Hotta, D. Trukhin, et al., Durvalumab plus platinum-etoposide versus platinum-etoposide in first-line treatment of extensive-stage small-cell lung cancer (CASPIAN): a randomised, controlled, open-label, phase 3 trial, Lancet 394 (10212) (2019) 1929–1939.
[6] M. Lu, R. Zhang, L.S. Qi, Y.L. Wang, X.X. Sun, J. You, Pathologic responses to neoadjuvant chemoimmunotherapy in primary limited-stage small-cell lung cancer, Thorac. Cancer 13 (22) (2022) 3208–3216.
[7] L. Wang, P. Wu, Z. Shen, Q. Yu, Y. Zhang, F. Ye, et al., An immune checkpoint-based signature predicts prognosis and chemotherapy response for patients with small cell lung cancer, Int. Immunopharmacol. 117 (2023), 109827.
[8] S. Ding, N. Qiao, Q. Zhu, Y. Tong, S. Wang, X. Chen, et al., Single-cell atlas reveals a distinct immune profile fostered by T cell-B cell crosstalk in triple negative breast cancer, Cancer Commun. (Lond., Engl.) (2023).
[9] M. Gryziak, K. Wozniak, L. Kraj, L. Rog, R. Stec, The immune landscape of hepatocellular carcinoma-where we are? Oncol. Lett. 24 (5) (2022) 410.
[10] M. Granai, L. Mundo, A.U. Akarca, M.C. Siciliano, H. Rizvi, V. Mancini, et al., Immune landscape in Burkitt lymphoma reveals M2-macrophage polarization and correlation between PD-L1 expression and non-canonical EBV latency program, Infect. Agents Cancer 15 (2020) 28.
[11] J. Sun, C. Yan, D. Xu, Z. Zhang, K. Li, X. Li, et al., Immuno-genomic characterisation of high-grade serous ovarian cancer reveals immune evasion mechanisms and identifies an immunological subtype with a favourable prognosis and improved therapeutic efficacy, Br. J. Cancer 126 (11) (2022) 1570–1580.
[12] C. Yan, K. Li, F. Meng, L. Chen, J. Zhao, Z. Zhang, et al., Integrated immunogenomic analysis of single-cell and bulk tissue transcriptome profiling unravels a macrophage activation paradigm associated with immunological and clinically distinct behaviors in ovarian cancer, J. Adv. Res 44 (2023) 149–160.
[13] Z. Zhang, L. Chen, H. Chen, J. Zhao, K. Li, J. Sun, et al., Pan-cancer landscape of T-cell exhaustion heterogeneity within the tumor microenvironment revealed a progressive roadmap of hierarchical dysfunction associated with prognosis and therapeutic efficacy, EBioMedicine 83 (2022), 104207.
[14] T. Li, T. Qiao, Unraveling tumor microenvironment of small-cell lung cancer: implications for immunotherapy, Semin. Cancer Biol. 86 (Pt 2) (2022) 117–125.
[15] B. Zhang, J. Wang, X. Wang, J. Zhu, Q. Liu, Z. Shi, et al., Proteogenomic characterization of human colon and rectal cancer, Nature 513 (7518) (2014) 382–387.
[16] D.J. Clark, S.M. Dhanasekaran, F. Petralia, J. Pan, X. Song, Y. Hu, et al., Integrated proteogenomic characterization of clear cell renal cell carcinoma, Cell 179 (4) (2019).
[17] L. Cao, C. Huang, D. Cui Zhou, Y. Hu, T.M. Lih, S.R. Savage, et al., Proteogenomic characterization of pancreatic ductal adenocarcinoma, Cell 184 (19) (2021).
[18] P. Micke, A. Faldum, T. Metz, K.M. Beeh, F. Bittinger, J.G. Hengstler, et al., Staging small cell lung cancer: veterans Administration Lung Study Group versus International Association for the Study of Lung Cancer–what limits limited disease? Lung Cancer 37 (3) (2002) 271–276.
[19] C.R. Merritt, G.T. Ong, S.E. Church, K. Barker, P. Danaher, G. Geiss, et al., Multiplex digital spatial profiling of proteins and RNA in fixed tissue, Nat. Biotechnol. 38 (5) (2020) 586–599.
[20] L. Ma, S. Heinrich, L. Wang, F.L. Keggenhoff, S. Khatib, M. Forgues, et al., Multiregional single-cell dissection of tumor and immune cells reveals stable lock-and-key features in liver cancer, Nat. Commun. 13 (1) (2022) 7533.
[21] X. Song, A. Xiong, F. Wu, X. Li, J. Wang, T. Jiang, et al., Spatial multi-omics revealed the impact of tumor ecosystem heterogeneity on immunotherapy efficacy in patients with advanced non-small cell lung cancer treated with bispecific antibody, J. Immunother. Cancer 11 (2) (2023).
[22] L. Jiang, J. Huang, B.W. Higgs, Z. Hu, Z. Xiao, X. Yao, et al., Genomic Landscape Survey Identifies SRSF1 as a Key Oncodriver in Small Cell Lung Cancer, PLoS Genet 12 (4) (2016), e1005895.
[23] J. George, J.S. Lim, S.J. Jang, Y. Cun, L. Ozretic, G. Kong, et al., Comprehensive genomic profiles of small cell lung cancer, Nature 524 (7563) (2015) 47–53.
[24] L. Cai, H. Liu, F. Huang, J. Fujimoto, L. Girard, J. Chen, et al., Cell-autonomous immune gene expression is repressed in pulmonary neuroendocrine cells and small cell lung cancer, Commun. Biol. 4 (1) (2021) 314.
[25] N. Roper, M.J. Velez, A. Chiappori, Y.S. Kim, J.S. Wei, S. Sindiri, et al., Notch signaling and efficacy of PD-1/PD-L1 blockade in relapsed small cell lung cancer, Nat. Commun. 12 (1) (2021) 3880.
[26] A. Bagaev, N. Kotlov, K. Nomie, V. Svekolkin, A. Gafurov, O. Isaeva, et al., Conserved pan-cancer microenvironment subtypes predict response to immunotherapy, Cancer Cell 39 (6) (2021) 845–865, e7.
[27] A. Liberzon, C. Birger, H. Thorvaldsdottir, M. Ghandi, J.P. Mesirov, P. Tamayo, The Molecular Signatures Database (MSigDB) hallmark gene set collection, Cell Syst. 1 (6) (2015) 417–425.
[28] T. Wu, E. Hu, S. Xu, M. Chen, P. Guo, Z. Dai, et al., clusterProfiler 4.0: a universal enrichment tool for interpreting omics data, Innov. (Camb.) 2 (3) (2021), 100141.
[29] S. Hanzelmann, R. Castelo, J. Guinney, GSVA: gene set variation analysis for microarray and RNA-seq data, BMC Bioinforma. 14 (2013) 7.
[30] G. Bindea, B. Mlecnik, H. Hackl, P. Charoentong, M. Tosolini, A. Kirilovsky, et al., ClueGO: a Cytoscape plug-in to decipher functionally grouped gene ontology and pathway annotation networks, Bioinformatics 25 (8) (2009) 1091–1093.
[31] M.D. Wilkerson, D.N. Hayes, ConsensusClusterPlus: a class discovery tool with confidence assessments and item tracking, Bioinformatics 26 (12) (2010) 1572–1573.
[32] D. Aran, Z. Hu, A.J. Butte, xCell: digitally portraying the tissue cellular heterogeneity landscape, Genome Biol. 18 (1) (2017) 220.
[33] D.S. Chen, I. Mellman, Elements of cancer immunity and the cancer-immune set point, Nature 541 (7637) (2017) 321–330.
[34] Y. Senbabaoglu, R.S. Gejman, A.G. Winer, M. Liu, E.M. Van Allen, G. de Velasco, et al., Tumor immune microenvironment characterization in clear cell renal cell carcinoma identifies prognostic and immunotherapeutically relevant messenger RNA signatures, Genome Biol. 17 (1) (2016) 231.
[35] Y. Zheng, Z. Chen, Y. Han, L. Han, X. Zou, B. Zhou, et al., Immune suppressive landscape in the human esophageal squamous cell carcinoma microenvironment, Nat. Commun. 11 (1) (2020) 6268.

[36] D.A. Braun, K. Street, K.P. Burke, D.L. Cookmeyer, T. Denize, C.B. Pedersen, et al., Progressive immune dysfunction with advancing disease stage in renal cell carcinoma, Cancer Cell 39 (5) (2021) 632–648, e8.
[37] Y. Sun, J. Xue, Expression profile and biological role of immune checkpoints in disease progression of HIV/SIV infection, Viruses 14 (3) (2022).
[38] P. Bankhead, M.B. Loughrey, J.A. Fernandez, Y. Dombrowski, D.G. McArt, P. D. Dunne, et al., QuPath: open source software for digital pathology image analysis, Sci. Rep. 7 (1) (2017) 16878.
[39] G. Esposito, G. Palumbo, G. Carillio, A. Manzo, A. Montanino, V. Sforza, et al., Immunotherapy in small cell lung cancer, Cancers 12 (9) (2020).
[40] W.Z. Wang, A. Shulman, J.M. Amann, D.P. Carbone, P.N. Tsichlis, Small cell lung cancer: subtypes and therapeutic implications, Semin Cancer Biol. 86 (Pt 2) (2022) 543–554.
[41] A. Gazdar, MS32.04 molecular phenotypes of SCLC, J. Thorac. Oncol. 13 (10) (2018).
[42] P.A. Ott, E. Elez, S. Hiret, D.-W. Kim, A. Morosky, S. Saraf, et al., Pembrolizumab in patients with extensive-stage small-cell lung cancer: results from the phase Ib KEYNOTE-028 study, J. Clin. Oncol. 35 (34) (2017) 3823–3829.
[43] M. Binnewies, E.W. Roberts, K. Kersten, V. Chan, D.F. Fearon, M. Merad, et al., Understanding the tumor immune microenvironment (TIME) for effective therapy, Nat. Med 24 (5) (2018) 541–550.
[44] Borczuk Aea. WHO Classification of tumors 5th Edition 2021 [Available from: https://www.who.int/.
[45] W. Wang, P. Hodkinson, F. McLaren, M.J. Mackean, L. Williams, S.E.M. Howie, et al., Histologic assessment of tumor-associated CD45(+) cell numbers is an independent predictor of prognosis in small cell lung cancer, Chest 143 (1) (2013) 146–151.
[46] S. Yang, W. Wei, Q. Zhao, B7-H3, a checkpoint molecule, as a target for cancer immunotherapy, Int J. Biol. Sci. 16 (11) (2020) 1767–1773.
[47] P. Khan, M. Fatima, M.A. Khan, S.K. Batra, M.W. Nasser, Emerging role of chemokines in small cell lung cancer: Road signs for metastasis, heterogeneity, and immune response, Semin Cancer Biol. 87 (2022) 117–126.
[48] D. Dangaj, M. Bruand, A.J. Grimm, C. Ronet, D. Barras, P.A. Duttagupta, et al., Cooperation between constitutive and inducible chemokines enables T cell engraftment and immune attack in solid tumors, Cancer Cell 35 (6) (2019).
[49] Y. Tang, Y. Hu, Y. Niu, L. Sun, L. Guo, CCL5 as a prognostic marker for survival and an indicator for immune checkpoint therapies in small cell lung cancer, Front Med (Lausanne) 9 (2022), 834725.
[50] K. Masuhiro, M. Tamiya, K. Fujimoto, S. Koyama, Y. Naito, A. Osa, et al., Bronchoalveolar lavage fluid reveals factors contributing to the efficacy of PD-1 blockade in lung cancer, JCI Insight 7 (9) (2022).
[51] C.-L. Hsu, D.-L. Ou, L.-Y. Bai, C.-W. Chen, L. Lin, S.-F. Huang, et al., Exploring markers of exhausted CD8 T cells to predict response to immune checkpoint inhibitor therapy for hepatocellular carcinoma, Liver Cancer 10 (4) (2021) 346–359.